N-Type Molecular Thermoelectrics Based on Solution-Doped Indenofluorene-Dimalononitrile: Simultaneous Enhancement of Doping Level and Molecular Order

Suhao Wang,* Huan Wei, Antoine Rillaerts, İbrahim Deneme, Michael Depriester, Suraj Manikandan, Jens Wenzel Andreasen, Abdelylah Daoudi, Sébastien Peralta, Stéphane Longuemart, Hakan Usta,* Jérôme Cornil,* Yuanyuan Hu,* and Wojciech Pisula*

The development of n-type organic thermoelectric materials, especially π-conjugated small molecules, lags far behind their p-type counterparts, due primarily to the scarcity of efficient electron-transporting molecules and the typically low electron affinities of n-type conjugated molecules that leads to inefficient n-doping. Herein, the n-doping of two functionalized (carbonyl vs dicyanovinylene) indenofluorene-based conjugated small molecules, 2,8-bis(5-(2-octyldodecyl)thien-2-yl)indeno[1,2-b]fluorene-6,12-dione (TIFDKT) and 2,2′-(2,8-bis(3-alkylthiophen-2-yl)indeno[1,2-b]fluorene-6,12-diylidene)dimalononitrile (TIFDMT) are demonstrated, with n-type dopant N-DMBI. While TIFDKT shows decent miscibility with N-DMBI, it can be hardly n-doped owing to its insufficiently low LUMO. On the other hand, TIFDMT, despite a poorer miscibility with N-DMBI, can be efficiently n-doped, reaching a respectable electrical conductivity of 0.16 S cm^{-1}. Electron paramagnetic resonance measurements confirm the efficient n-doping of TIFDMT. Based on density functional theory (DFT) calculations, the LUMO frontier orbital energy of TIFDMT is much lower, and its wave function is more delocalized compared to TIFDKT. Additionally, the polarons are more delocalized in the n-doped TIFDMT. Remarkably, as indicated by the grazing-incidence wide-angle X-ray scattering (GIWAXS), the molecular order for TIFDMT thin-film is enhanced by n-doping, leading to more favorable packing with edge-on orientation and shorter π-π stacking distances (from 3.61 to 3.36 Å). This induces more efficient charge transport in the doped state. Upon optimization, a decent thermoelectric power factor of 0.25 µWm^{-1}K^{-2} is achieved for n-doped TIFDMT. This work reveals the effect of carbonyl vs dicyanovinylene on the n-doping efficiency, microstructure evolution upon doping and thermoelectric performance, offering a stepping stone for the future design of efficient n-type thermoelectric molecules.

1. Introduction

To address environmental issues caused by fossil fuels and meet the growing energy demands of humanity, scientists have been searching for renewable and green energy sources. In line with this quest, there has been a surge of interest in thermoelectric (TE) technology, which sustainably harvests waste heat and converts it into useful electrical energy.[1] Although inorganic semiconductors have been studied for decades as efficient TE materials, their widespread use is limited due to their scarcity, toxicity, rigidity, and the energy-intensive processing they require. Emerging as new-generation TE materials, organic semiconductors have gained enormous interest thanks to their unique properties,[2] such as intrinsically low thermal conductivity,[3] potentially low production costs, environmental friendliness,[2b] flexibility,[4] stretchability,[5] diverse chemical synthesis,[6] solution processability (e.g., printability),[7] and a wide range of applications.[2f,8] Among organic thermoelectric (OTE) materials, π-conjugated polymers[9] have recently shown remarkable progress in molecular design[10] and the high performance of doped thin films.[11] π-conjugated small molecules,

S. Wang, M. Depriester, A. Daoudi, S. Longuemart
Unité de Dynamique et Structure des Matériaux Moléculaires
Université du Littoral Côte d'Opale
145 Avenue Maurice Schumann, Dunkerque 59140, France
E-mail: suhao.wang@univ-littoral.fr

H. Wei, Y. Hu
Changsha Semiconductor Technology and Application Innovation
Research Institute & International Science and Technology Innovation
Cooperation Base for Advanced Display Technologies of Hunan Province
College of Semiconductors (College of Integrated Circuits)
Hunan University
Changsha 410082, China
E-mail: yhu@hnu.edu.cn

**ADVANCED
SCIENCE NEWS**

www.advancedsciencenews.com

**ADVANCED
MATERIALS
TECHNOLOGIES**

www.advmattechnol.de

on the other hand, are typically simpler to purify and crystallize. They have uniform and controllable molecular weights, and their synthesis offers good batch-to-batch reproducibility.[12] Moreover, molecular thin-film microstructures and morphologies can be predicted by using advanced models.[13] Despite these advantages and unique potential directions, the development of molecular thermoelectrics has received less attention compared to other types of OTE materials. Specifically, the development of n-type molecular thermoelectrics lags substantially behind their p-type counterparts,[2g,14] which is similar to the situation in n-type[15] versus p-type polymeric materials.[16] This is because efficient electron-transporting molecular semiconductors are scarce, and their insufficiently low electron affinities typically result in ineffective n-doping.[17]

One of the pioneering works on n-doping of organic small molecules involves doping of [6,6]-phenyl C61 butyric acid methyl ester (PCBM) with 4-(1,3-dimethyl-2,3-dihydro-1H-benzoimidazol-2-yl)phenyl (N-DMBI), resulting in a conductivity of 1.9×10^{-3} S cm^{-1}.[18] Following this initial study, N-DMBI has become a benchmark n-type dopant in the field of organic semiconductors. According to another earlier report, perylene diimide (PDI) is self-dopable by having a charged doping group that is intrinsically bonded to the π-conjugated core, reaching a conductivity of 10^{-3} S cm^{-1}.[19] In a later study, by modifying the side chain length in PDIs, both film morphology and electronic properties were tuned, and significantly higher conductivities of 0.01 and 0.4 S cm^{-1} were achieved with four and six methylene spacer groups, respectively.[20] Recently, three n-type small molecules based on naphthalene bis-isatin π-core were synthesized and doped with N-DMBI, with the best molecule yielding conductivities of up to 0.97 S cm^{-1}.[21] As another example, an indandione-terminated small molecule was very recently doped with both N-DBMI and Leuco crystal violet (LCV) dopants, which resulted in conductivities of 0.014 and 0.072 S cm^{-1}, respectively.[22] N-doped

π-conjugated small molecules generally exhibit conductivities of less than 0.1 S cm^{-1}, with the exception of a small number of candidates that showed n-type conductivities of up to 10 S cm^{-1}.[23] The low conductivity values achieved with n-type small molecules to date may be attributed to their low electron mobilities, shallow electron affinities, and poor miscibility with dopants.[14] Despite these recent advances, which span only a limited number of n-type molecular structures, understanding the n-doping of π-conjugated molecules for organic thermoelectrics and elucidating the structure-property-performance relationships remains very important.

Herein, we report the n-doping of two π-conjugated small molecules, 2,8-bis(5-(2-octyldodecyl)thien-2-yl)indeno[1,2-b]fluorene-6,12-dione (TIFDKT) and 2,2′-(2,8-bis(3-alkylthiophen-2-yl)indeno[1,2-b]fluorene-6,12-diylidene)dimalononitrile (TIFDMT), with N-DMBI (**Figure 1**). The two small molecules studied herein were synthesized in accordance with the previously reported synthesis and purification methods.[24] TIFDKT and TIFDMT were specifically chosen for thermoelectrics based on their highly favorable structural and electronic properties. First, both molecules include a donor-acceptor-donor type of π-backbone with long, linear (-C$_{12}$H$_{25}$) alkyl substituents. This is critical to achieve solution-processability and proper molecular ordering in thin film. Second, the dicyanovinylene versus carbonyl comparison is crucial to better understand the effect of functional groups on designing molecular thermoelectric materials. The functional groups have been placed on the indenofluorene unit in a symmetric fashion to achieve a π-system extending to both ends of the indenofluorene unit along the short-axis. Third, we specifically design the π-system with dicyanovinylenes (in TIFDMT) to ensure a more stabilized Lowest Unoccupied Molecular Orbital (LUMO) energy level with an extended orbital wave function (i.e., enhanced mesomeric effect), whereas these characteristics remain more limited (i.e., relatively higher and less π-extended LUMO) with carbonyls (in TIFDKT). By measuring cyclic voltammograms in dichloromethane, the Highest Occupied Molecular Orbital (HOMO) /LUMO frontier orbital energy levels are estimated as −5.62 eV/−3.60 eV for TIFDKT and −5.65 eV/−4.12 eV for TIFDMT (Figure S1, Supporting Information). Notably, TIFDMT exhibits high electron mobilities of over 0.1 cm^2 V^{-1} s^{-1} in solution-processed organic field-effect transistors.[24a,25] Finally, incorporating dicyanovinylene units into indenofluorenes is synthetically straightforward, as compared with the introduction of some other electron-withdrawing units (e.g., -NO$_2$ and -F), through Knoevenagel condensations. In this current work, it is discovered that although TIFDMT is poorly miscible with the dopant, it shows in the n-doped state a several orders of magnitude higher conductivity as compared to the carbonyl-functionalized TIFDKT. Electron spin resonance (ESR) and UV–vis measurements prove that the n-doping level of TIFDMT is significantly higher than that of TIFDKT. DFT calculations indicate a significant energy difference between the LUMOs of the two molecules and reveal that polarons are more delocalized over the molecular π-backbone in n-doped TIFDMT. Interestingly, the molecular ordering for the TIFDMT thin-film is enhanced by n-doping, as characterized by grazing-incidence wide-angle X-ray scattering (GIWAXS). By revealing the impact of carbonyl versus dicyanovinylene on the n-doping efficiency,

A. Rillaerts, J. Cornil
Service de Chimie des Matériaux Nouveaux
Université de Mons
Mons B-7000, Belgium
E-mail: jerome.cornil@umons.ac.be

İ. Deneme, H. Usta
Department of Materials Science and Nanotechnology Engineering
Abdullah Gül University
Kayseri 38080, Türkiye
E-mail: hakan.usta@agu.edu.tr

S. Manikandan, J. W. Andreasen
Department of Energy Conversion and Storage
Technical University of Denmark
Kgs. Lyngby 2800, Denmark

S. Peralta
Laboratoire de Physicochimie des Polymères et des Interfaces
CY Cergy Paris Université
5 Mail Gay Lussac, Neuville-sur-Oise 95000, France

W. Pisula
Max Planck Institute for Polymer Research
Ackermannweg 10, 55128 Mainz, Germany
E-mail: pisula@mpip-mainz.mpg.de

W. Pisula
Department of Molecular Physics
Faculty of Chemistry
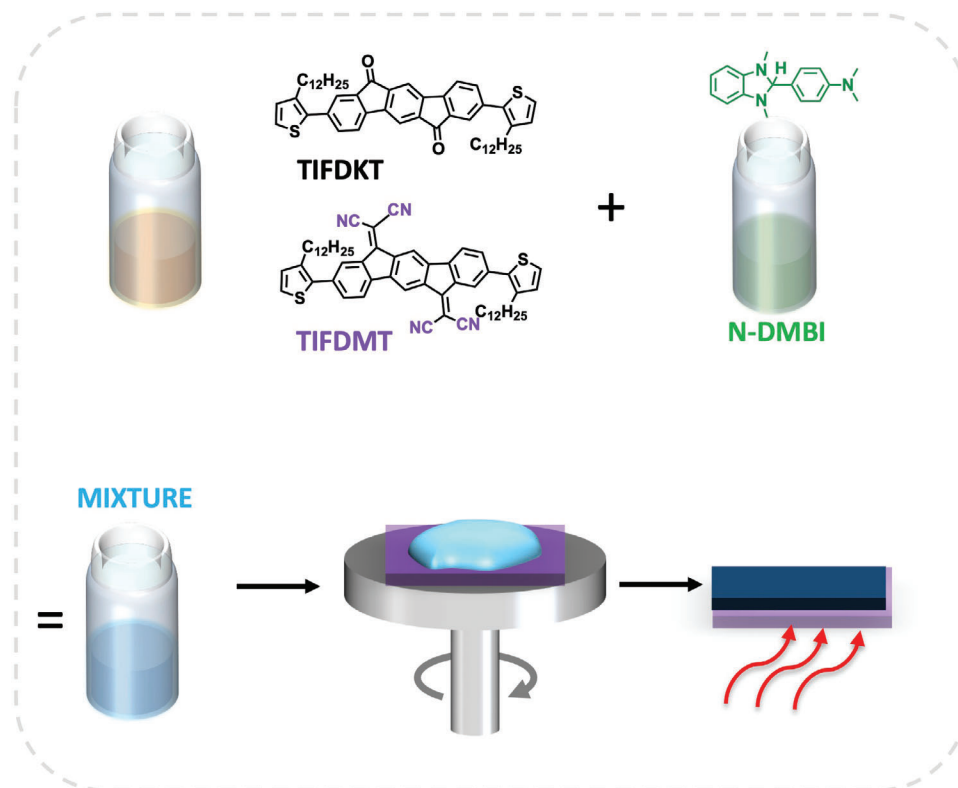Lodz University of Technology
Zeromskiego 116, Lodz 90-924, Poland

ADVANCED
SCIENCE NEWS

www.advancedsciencenews.com

ADVANCED MATERIALS
TECHNOLOGIES

www.advmattechnol.de

Figure 1. Molecular structures of TIFDKT and TIFDMT, and the illustration of mix-solution doping methods.

microstructure evolution upon doping, and thermoelectric performance, this work highlights the importance of simultaneous enhancement of molecular ordering and doping level of n-type π-conjugated small molecules for the future design of efficient thermoelectrics.

2. Results and Discussion

The evolution of the electrical conductivity for TIFDKT and TIFDMT thin films was recorded as a function of the N-DMBI molar ratio, as shown in **Figure** 2A. The conductivities of the pristine TIFDKT and TIFDMT thin films are comparable, both on the order of 10^{-6} S cm^{-1}. After doping, the conductivity for the TIFDKT thin film remains almost unchanged, even at a dopant concentration of 20 mol%. By contrast, the conductivity of the TIFDMT thin film increases by 3 orders of magnitude with a low dopant concentration of 3 mol%, reaching 2.1×10^{-3} S cm^{-1}. The conductivity continues to gradually raise with the increased dopant concentration, and the highest conductivity value of 0.16 S cm^{-1} is achieved with the dopant concentration of 20 mol%. As the dopant concentration further increases above 20 mol%, the conductivity of the TIFDMT thin film decreases, which is commonly observed as a result of the disruption of thin-film microstructure by excessive dopants.[21] Based on the temperature-dependent conductivity measurements carried out on the 20 mol% N-DMBI-doped TIFDMT thin film (Figure 2B), the activation energy (EA) is determined to be as low as 0.087 eV, suggesting a highly ordered molecular packing for TIFDMT molecules in the doped thin-film state.

We performed electron spin resonance (ESR) measurements on the doped TIFDKT and TIFDMT thin films (Figure 2C). While no noticeable signal is recorded for the doped TIFDKT thin film even at a doping concentration of 20 mol%, strong ESR signals are observed for the doped TIFDMT thin film starting from low doping concentrations and becoming stronger as the doping concentration increases. This confirms the successful doping of TIFDMT thin films and the formation of polarons in the molecular lattice.[26] As shown in Figure 2D, the double integral of the ESR signals for the N-DMBI-doped TIFDMT thin films increases by approx. two orders of magnitude as the doping level rises, eventually saturating at 20 mol%. The spin density in the doped TIFDMT films is estimated by referring to a standard sample of (2,2,6,6-tetramethylpiperidin-1-yl)oxyl (TEMPO) in toluene with known spin density based on the assumption that each TEMPO molecule has one spin, and the experimental setting parameter and the Q-factor of the resonator should be taken into account, as proposed by Neher et al.[27] It is apparent that N-DMBI induces more spins (i.e., unpaired electrons or polarons) with increasing doping concentration, which is consistent with the evolution of the electrical conductivity as shown in Figure 2A. The number of spins for different doping concentrations is shown in Figure 2E. The polaron generation efficiency (ηi) is typically defined as the ratio of the number of polarons (spins) to the number of dopants, which represents the efficiency of a dopant to generate polarons. ηi is a crucial metric for assessing the doping capability of a dopant for a particular semiconductor.[28] Considering that not all induced polarons eventually become free carriers, it is noteworthy that ηi is typically higher than the doping

**ADVANCED
SCIENCE NEWS**

www.advancedsciencenews.com

**ADVANCED
MATERIALS
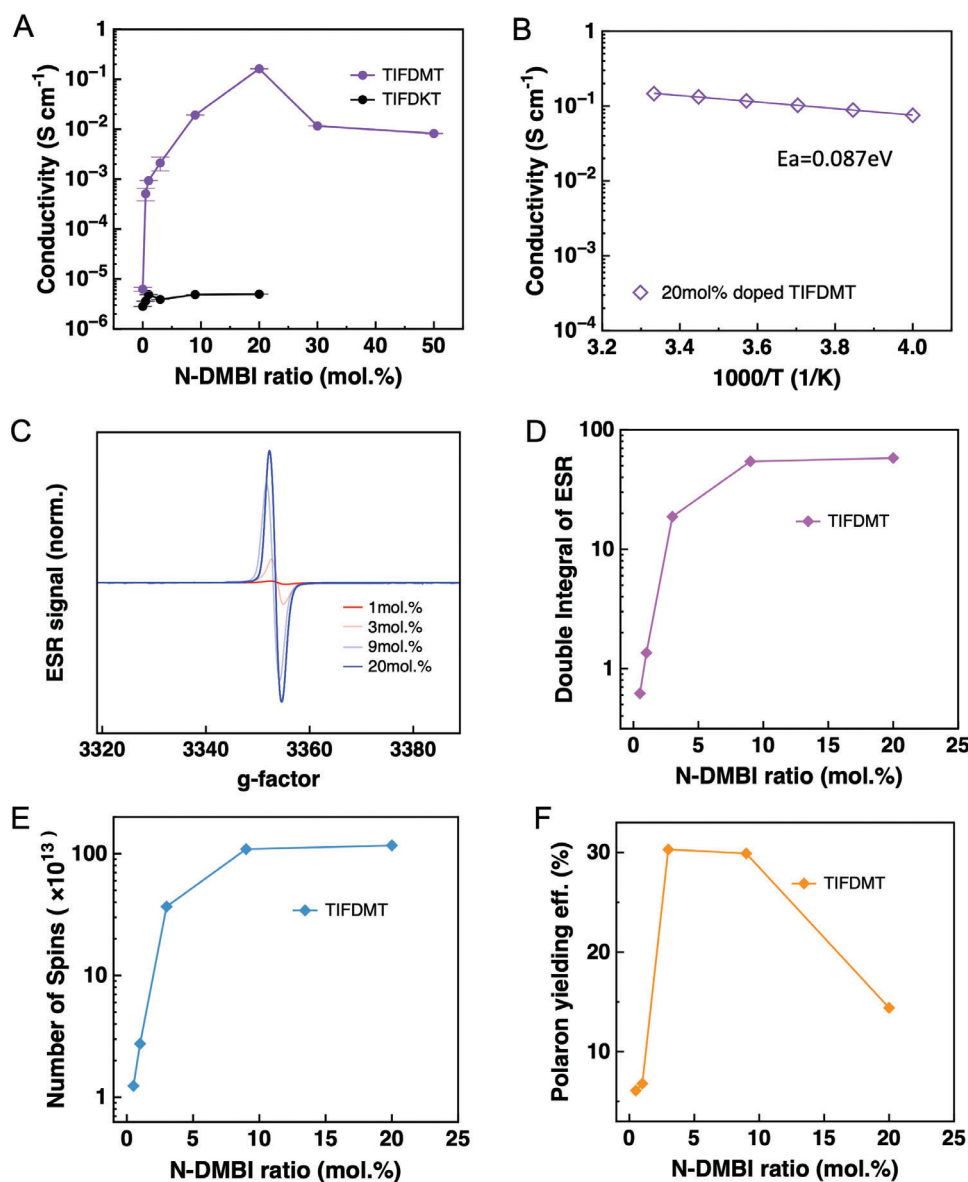TECHNOLOGIES**

www.advmattechnol.de

Figure 2. A) Electrical conductivity of the pristine and the doped TIFDKT and TIFDMT thin films as a function of N-DMBI dopant concentration. B) Temperature dependence of the electrical conductivity of the 20 mol% doped TIFDMT thin film. C) ESR spectroscopy of the N-DMBI-doped TIFDMT thin films for different doping concentrations measured at room temperature. D) Double integral of the ESR signals, E) the number of spins and F) the polaron generation efficiency of the N-DMBI-doped TIFDMT thin film as a function of doping concentration.

efficiency.[29] Figure 2F shows the η_i values of the N-DMBI-doped TIFDMT thin films. Although the number of spins continues to increase up to 20 mol% of doping concentration, the maximum η_i of 30.3% is obtained for the 3 mol% N-DMBI-doped TIFDMT film. This is likely due to the formation of dopant aggregations at higher dopant concentrations (see below) leading to a lower η_i value.

DFT calculations are employed to shed light on the geometric and electronic properties of the two molecules in their neutral and negatively charged states. As shown in Figure S2 (Supporting Information), both molecules show a rigid, coplanar indenofluorene π-conjugated core with two thiophenes on both sides. The geometry of the two molecules enables thiophene

rotation along the carbon-carbon single bonds to give dihedral angles of $\approx 45°$. The alkyl side chain is represented here by a methyl group to save computational time. The dihedral angles are marginally affected in their negatively charged states. As shown in Figure S3 (Supporting Information), the HOMO is fully delocalized on both molecules but bears no electronic density on the electroactive functionalities. The HOMO energy level of TIFDMT is stabilized by 0.12 eV compared to that of TIFDKT; these very similar values are consistent with the CV data. In contrast, LUMO is centered only on the indenofluorene core including the functional groups, as a result of their strong electron-withdrawing characteristics, as well as the large twists of the external thiophene rings. The LUMO energy level of TIFDMT is
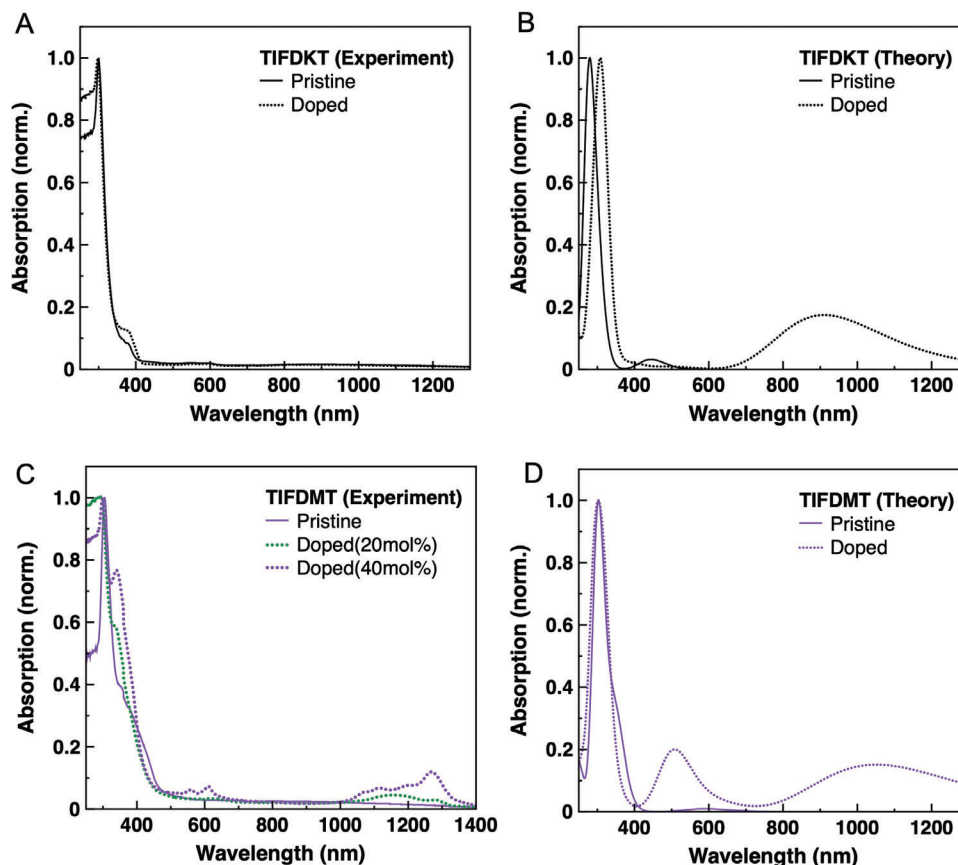
Figure 3. UV–vis–NIR absorption spectra of A) TIFDKT and C) TIFDMT films in both pristine and charged electronic states. TD-DFT simulated absorption spectra of B) TIFDKT and D) TIFDMT in the gas phase.

stabilized by 1.17 eV compared to that of TIFDKT, which follows the same trend as experimentally indicated by CV measurements and rationalizes that TIFDMT is more easily n-doped than TIFDKT. Although the calculated values of HOMO and LUMO cannot be directly compared with the experimental values since they are calculated for an isolated molecule in the gas phase at 0 K, the calculated energy difference between frontier levels has significance.[30] The remarkably higher electrical conductivity of TIFDMT can be well explained by its significantly lower LUMO energy level. Such a huge effect of LUMO energy level on the doped performance of OSCs was previously reported in polymeric systems, such as organoboron polymers.[31] Since N-DMBI is a hydride donor,[32] the doping probably takes place directly via hydride H⁻ transfer,[33] and this is even more likely in polar media (i.e. chloroform).[34]

UV–vis–NIR absorption spectroscopy was performed to understand the optical properties of TIFDKT and TIFDMT films both before and after doping. As shown in **Figure 3A**, there is little difference in the optical properties of pristine and 20 mol% doped TIFDKT, indicating that TIFDKT can be hardly n-doped by N-DMBI. This is consistent with the ESR-silent feature of the 20mol% doped TIFDKT. In contrast, polaron bands arise in the 20mol% and 40mol% doped TIFDMT (Figure 3C), suggesting that the n-doping of TIFDMT was successful. After exposing the 40mol% doped TIFDMT in the air for just 5min, the polaron

bands drop substantially (Figure S4, Supporting Information). Note that n-doped organic semiconductors typically suffer from poor air stability,[35] due to the instability of both n-type organic semiconductors/dopants and negative polarons.[36] The solving of this issue relies on the rational design of organic semiconductors and dopants,[37] as well as the development of novel doping approaches.[11d,17a,37] TD-DFT calculations well replicate the experimental features as the main peak of the neutral form is located in the same wavelength region. Notably, the two subgap absorption features of doped TIFDMT show up in the same energy range as in the theoretical simulations. Note that the exact shape of the experimental absorption band could not be fully reproduced by DFT since the employed calculations herein only take into account one molecule without vibronic couplings. Full width at mid height (FWMH) cannot be compared since it is arbitrarily defined in the simulations to match the experimental resolution. The similar intensity of the two polaronic subgap features observed in both cases also support the formation of polarons.

Since electrons are paired in neutral systems (i.e., no unpaired electrons), the sum for the atomic spin density (ρ_α-ρ_β) amounts to zero wherever in space, which is not the case in an open-shell anionic system. **Figure 4A,B** represent the distributions of spin density for both n-doped small molecules, in which the colored code reflects the localization of the unpaired electron. The atoms highlighted in green support the highest spin density while the
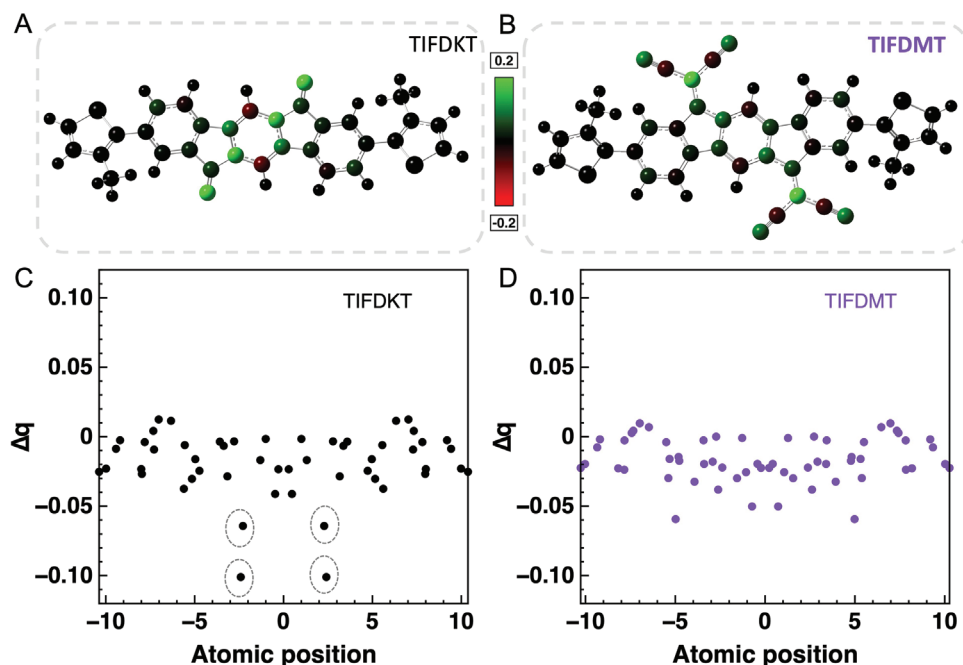
**ADVANCED
SCIENCE NEWS**

www.advancedsciencenews.com

**ADVANCED
MATERIALS
TECHNOLOGIES**

www.advmattechnol.de

Figure 4. DFT-calculated electronic spin densities in n-doped TIFDKT A) and TIFDMT B) molecules, and the corresponding Mulliken charge distributions (C and D, respectively, dash circles highlight undesirable charge localization in TIFDKT).

dark zones are the regions with all spins paired up. In TIFDKT, spin density is mostly localized on the central benzene ring and the two carbonyl functionalities, whereas the spin density distribution is more extended in TIFDMT by delocalizing over the dicyanovinylene bridges. This analysis can be complemented by the corresponding Mulliken charge distributions (Figure 4C,D), which are obtained by subtracting the Mulliken atomic charges of the charged system from those characteristics for the neutral system. A Mulliken population analysis allows for casting down the total electronic density into atomic charges to assess where there is a depletion or accumulation of electrons. Herein, we report the difference between the atomic charges in the neutral versus singly doped state in order to visualize the localization of the positive charge induced by doping (i.e., on the atoms highlighted in green). While the TIFDKT π-backbone concentrates a significant amount of charge at the center, TIFDMT exhibits a more uniform charge distribution along the π-backbone, which should facilitate the desired charge transfer between TIFDMT molecules in the thin-film phase. The undesirable charge localization in TIFDKT is clearly seen as the location of the four largest negative charges over the central part of the π-backbone in Figure 4C.

To understand the change of the morphology upon doping, tapping mode atomic force microscopy (AFM) was performed on both pristine and doped films of TIFDKT and TIFDMT. As shown in **Figure 5A**, the pristine TIFDMT film displays multilayers with an uncontinous top layer. After doping, the layers become more continuous, whereas dopant aggregates appear on the top of the film (Figure 5B), suggesting poor miscibility between TIFDMT and N-DMBI. By contrast, there is no distinct change of the morphology for TIFDKT before and after doping (Figure S5A,B, Supporting Information), indicating a good miscibility between TIFDKT and N-DMBI, which could be ascribed to the better sol-

ubility of the carbonyl-functionalized indenofluorene π-system. To gain information about the influence of doping on the microstructure and molecular packing of TIFDMT, 2D grazing-incidence wide-angle X-ray scattering (GIWAXS) measurements were performed for the pristine and 20 mol% N-DMBI-doped thin films. Interestingly, the patterns in Figure 5C,D and line-cut in Figure S6 (Supporting Information) indicate significant changes in the molecular arrangement and the crystallinity upon doping. The out-of-plane reflections are related to a layer organization, which is present for both thin films but with different d-spacing values as derived from the main scattering intensity. The layer d-spacing is reduced from 31.4 to 25.0 Å by the incorporation of the N-DMBI dopant. At the same time, the overall crystallinity for the doped thin film is increased as implied by the observed smaller full-width-at-half-maximum (fwhm) values of the sharper reflections. The molecular packing is also significantly affected by n-doping. The GIWAXS patterns clearly showed that the location of the corresponding π-stacking reflection shifts from off-meridional to in-plane for doped TIFDMT. While the pristine TIFDMT molecules reveal a π-stacking distance of 3.61 Å and arrange in a tiled fashion on the surface as illustrated in Figure 5E, in the doped state the π-stacking distance decreases to 3.36 Å adopting an edge-on dominant orientation on the surface (Figure 5F). The observed d-spacing along with the in-plane π-stacking interactions clearly suggest that TIFDMT molecules adopt an edge-on layer packing with alkyl chain interdigitations in the n-doped thin-film state.[24a] There is no evidence that the dopants intercalate into the π–π stacks of TIFDMT. Rather, the dopants form aggregates on top of the TIFDMT film, as indicated by the AFM image. As suggested by previously reported DFT calculations, the polaron delocalizes between neighboring molecular backbones resulting in attractive forces that
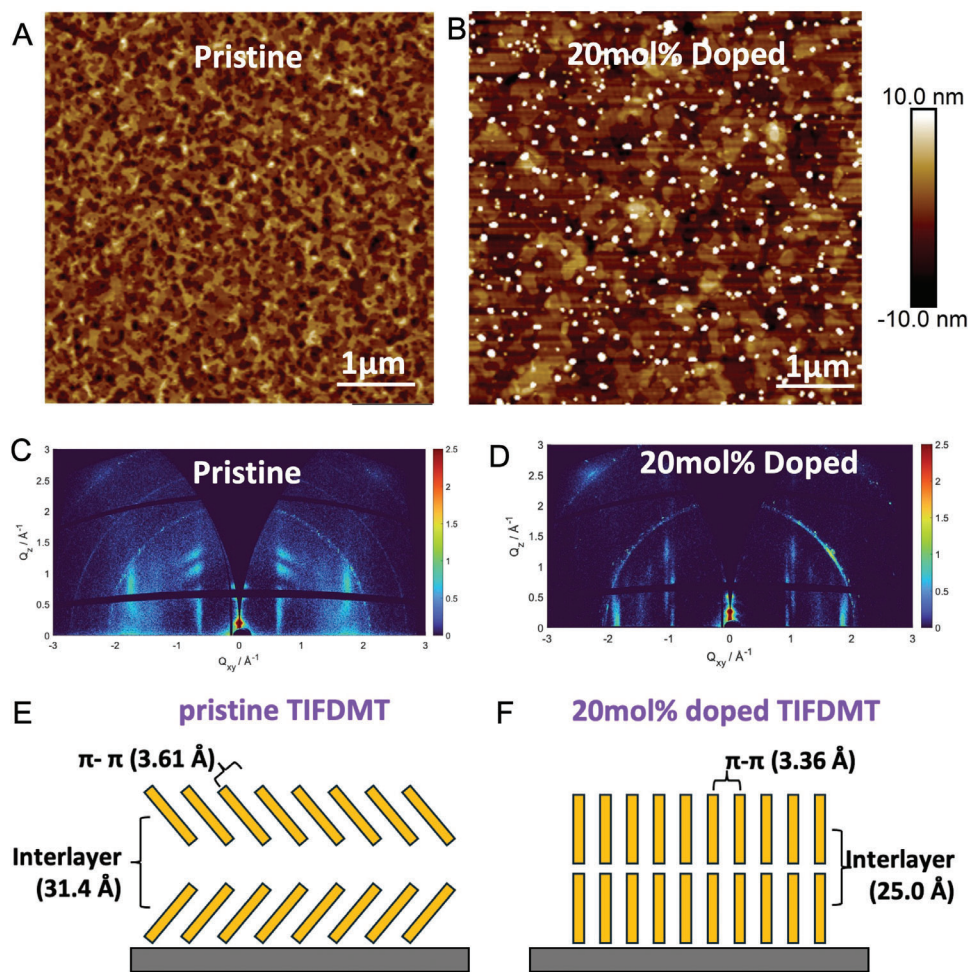
**ADVANCED
SCIENCE NEWS**

www.advancedsciencenews.com

**ADVANCED
MATERIALS
TECHNOLOGIES**

www.advmattechnol.de

Figure 5. AFM tapping mode images of the pristine A) and the 20 mol% doped B) TIFDMT thin films. 2D GIWAXS patterns of the pristine C) and the 20 mol% doped D) TIFDMT thin films. Schematic illustration of the molecular packing for the pristine E) and the 20 mol% doped F) TIFDMT thin films. The yellow rectangles represent the TIFDMT molecular structures along its short π-molecular axis, forming a layer packing with alkyl chain interdigitations in the out-of-plane direction.

decrease the π–π distance.[38] Such a phenomenon has been observed in the doping of conjugated polymers.[11b,39] Notably, the tighter packing and especially reduced π-stacking distance are important factors for more efficient charge transport.[11b,40] As reported by Kim et al, highly ordered microstructures were formed after doping of a conjugated polymer using a novel solvent combination doping method, leading to an increase of charge carrier mobility by over three orders of magnitude compared to that of the pristine film. Similarly, the better molecular order and shorter π-stacking distance herein well explain the significantly improved conductivity in the n-doped TIFDMT thin film.[11b] On the other hand, there is no obvious change in the microstructure of TIFDKT before and after doping (Figure S7, Supporting Information), primarily due to the lack of polaron formation regardless of its host-dopant miscibility.

To assess the potential of TIFDMT in OTE devices, we evaluated the thermoelectric performance of N-DMBI-doped TIFDMT thin-films. The Seebeck coefficient (S) is determined by applying a temperature gradient across the doped thin film and monitoring the thermovoltages. The measured S values of TIFDMT films with different doping concentrations are presented in **Figure 6A**. In theory, the S value is influenced by the difference between the Fermi level energy (E_F) and the charge transport energy (E_T).[41] As the doping level rises, more charges are created, shifting E_F toward E_T and altering the absolute S value. Indeed, the S value of the N-DMBI-doped TIFDMT thin-films changes from −355 to −123 μV K^{-1} by increasing the doping concentration from 3 to 20 mol%. The power factor (PF) is a crucial statistic for characterizing thermoelectric performance, which is dependent on the interplay between σ and S. Using the acquired σ and S values, the PF values can be calculated from $PF = S^2\sigma$, see Figure 6B, where the N-DMBI-doped TIFDMT thin-film reveals an optimized PF of 0.25 ± 0.006 μWm^{-1}K^{-2} at a doping concentration of 20 mol%.

3. Conclusion

In conclusion, two π-conjugated small molecules TIFDKT and TIFDMT were n-doped by N-DMBI for the first time, and the impact of carbonyl versus dicyanovinylene units on doping efficiency, thin-film microstructure and thermoelectric performance
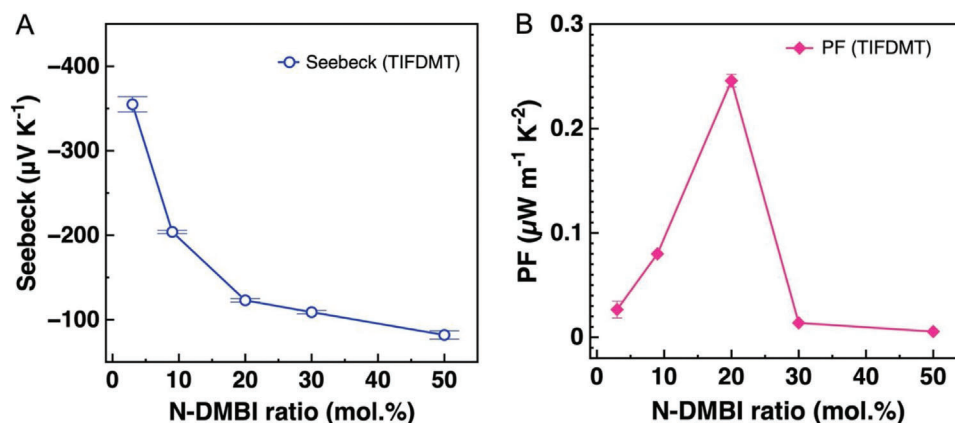
**ADVANCED
SCIENCE NEWS**

www.advancedsciencenews.com

**ADVANCED
MATERIALS
TECHNOLOGIES**

www.advmattechnol.de

Figure 6. A) Seebeck coefficient and B) power factor of n-doped TIFDMT films as a function of dopant concentration.

was systematically investigated. Owing to its polar carbonyl groups and higher solubility, TIFDKT exhibits good miscibility with the polar dopant molecule N-DMBI. However, because of its inadequately low LUMO, the n-doping of TIFDKT remains inefficient. Promisingly, TIFDMT with a significantly deeper LUMO can be effectively n-doped to achieve a respectable electrical conductivity of > 0.1 S cm^{-1} despite its lower miscibility with N-DMBI. The significant energy difference between the LUMOs of the two compounds is confirmed by DFT calculations, which also demonstrate that the polarons in the n-doped TIFDMT are more delocalized. Measurements of electron paramagnetic resonance provide further credence to the efficient n-doping of the dicyanovinylene-based TIFDMT. The GIWAXS results show that the doping significantly improves the molecular order of TIFDMT, resulting in a reorganization and closer edge-on π–π stacking distance, which promotes more effective charge transport in the doped state. In the evaluation of the thermoelectric properties, a respectable thermoelectric power factor of 0.25 μWm^{-1}K^{-2} is attained for n-doped TIFDMT. Higher thermoelectric performance may be achievable by introducing polar side chains (e.g. ethylene glycol) facilitating an enhanced molecule-dopant miscibility,[42] and/or by applying dopants with smaller size leading to less disruption of the film microstructure at high dopant concentrations.[43] Our results demonstrate that functionalized indenofluorenes with stabilized and delocalized frontier molecular orbitals are promising candidates for solution-processable n-type thermoelectric materials and sustainable energy solutions.

4. Experimental Section

Mixed-Solution Doping: The organic semiconductor solutions were prepared by dissolving the small molecular solids in chloroform at a concentration of 10.0 mg mL^{-1}. The dopant solution was prepared by dissolving n-DMBI solid in chloroform to yield a concentration of 5 mg mL^{-1}. The two solutions were blended in accordance with the intended doping ratio to create the doped solutions. where the two abovementioned solutions were mixed in different volume ratios.

Film Preparation and Electrical Measurements: First, photolithography and heat evaporation were used to create electrodes on Si substrates with 300 nm SiO$_2$ that included 2 nm chromium and 30 nm gold. Second, the

substrate was ultrasonically cleaned for one minute each in deionized water, acetone, and isopropanol. After that, the substrate received a 15-min UV/ozone treatment. Following that, the substrate was altered by octadecyltrichlorosilane (ODTS) in a vacuum oven for 120 min at 120 °C. Chloroform, hexane, and isopropanol were then used in consecutive order for one minute of cleaning. Lastly, the substrate was spin-coated with the organic semiconductor solution for 20 s at 1500 rpm min^{-1}, followed by a 30 min annealing process at temperatures over 100 °C. Four-probe electrical conductivity (L/W = 160 μm/1000 μm with two fingers spaced 40 μm apart) was measured using a Keithley 4200 semiconductor analyzer inside glovebox.

ESR Measurements: The produced doping solutions were put into paramagnetic tubes for ESR measurement, and the solvent was removed by drying them in a glove box filled with Ar. The ESR spectra were recorded at room temperature using a JEOL JES-FA200 ESR spectrometer following the sealing of the paramagnetic tubes.

DFT Calculations: The functional used for all calculations is LCω-HPBE with a 6–31G(d,p) basis set. This long-range corrected functional was chosen because the description of the charge distribution is improved thanks to the introduction of an exact Hartree Fock exchange term[44] to depict long-range electronic interactions and due to the possibility to tune the ω cut-off value separating the short from long range. This tuning is performed on geometrically optimized systems by minimizing the difference between ionization potential (IP) and HOMO energy; and electronic affinity (EA) and LUMO energy. Koopmans theorem defines the HOMO of the neutral molecule as the IP and the LUMO as the EA. IP is exactly defined as the energy difference between the neutral and cationic system while EA is defined as the energy difference between anionic and neutral systems. The 6–31G(d,p) basis set offers a good compromise between computational cost and accuracy. The calculations are performed in gas phase at 0 K and with the alkyl sidechain replaced by a methyl group to reduce the calculation time. No counter-ions are involved in the calculations on charged systems. The absorption spectra have been simulated at the Time-dependent (TD-) DFT level using the same functional and basis set.[45]

UV–Vis–NIR: The UV–vis–NIR absorption spectra of the films were performed using UV-3600PLUS (SHIMADZU).

GIWAXS Measurements: A laboratory setup was used (Xeuss 3.0 from Xenocs S.A.). A microfocus copper source was used to focus and monochromatize Cu Kα radiation (wavelength (λ) = 1.5418 Å) using a 2D single reflection multilayer optic and scatterless slits. The silicon substrate surface was oriented with a grazing incidence angle of 0.18° to the entering X-ray beam. The dispersed X-rays were detected using an Eiger 4M single-photon counting detector with 75 μm pixels (DECTRIS) located 80.0 mm from the sample.

AFM Measurements: The surface morphology of polymer films was measured using atomic force microscopy on Icon coupled at Nanoscope

V controller from Bruker in the Tapping mode. The probe was a ScanAsyst Air (Bruker) with a spring constant of 0.4 N m^{-1}.

Seebeck Coefficient Measurements: To determine the Seebeck coefficient of the doped samples, a homemade thermoelectric testing equipment was employed. The devices, which include one heater and two thermometers that also function as electrical contacts, were created by photolithographically patterning Cr (10 nm) and Au (15 nm) metal bilayers on glass substrates. To obtain Seebeck coefficient $S = \frac{\Delta V}{\Delta T}$, the temperature gradient between the two electrodes was determined by translating the resistance of electrodes into temperature using the temperature-coefficient-of resistance (TCR), and the built-in thermal voltage was measured using Keithley nanovoltmeter model 2182A. All Seebeck coefficients were measured at 300 K in high vacuum ($<10^{-5}$ mbar) using Janis ST-100.

Statistical Analysis: Electrical and Seebeck coefficient measurements were repeated on three samples and then statistically analyzed to get mean values and SD. The data are presented as mean $\pm$ standard deviation (mean $\pm$ SD). Origin was used for statistical analysis.

Supporting Information

Supporting Information is available from the Wiley Online Library or from the author.

Conflict of Interest

The authors declare no conflict of interest.

Data Availability Statement

The data that support the findings of this study are available from the corresponding author upon reasonable request.

[1] a) D. Beretta, N. Neophytou, J. M. Hodges, M. G. Kanatzidis, D. Narducci, M. Martin- Gonzalez, M. Beekman, B. Balke, G. Cerretti, W. Tremel, A. Zevalkink, A. I. Hofmann, C. Müller, B. Dörling, M. Campoy-Quiles, M. Caironi, *Mater. Sci. Eng. R Rep.* **2019**, *138*, 100501; b) P. A. Finn, C. Asker, K. Wan, E. Bilotti, O. Fenwick, C. B. Nielsen, *Front. Electr. Mater.* **2021**, *1*, 677845.

[2] a) B. Russ, A. Glaudell, J. J. Urban, M. L. Chabinyc, R. A. Segalman, *Nat. Rev. Mater.* **2016**, *1*, 16050; b) Q. Zhang, Y. Sun, W. Xu, D. Zhu, *Adv. Mater.* **2014**, *26*, 6829; c) Y. Chen, Y. Zhao, Z. Liang, *Energy Environ. Sci.* **2015**, *8*, 401; d) M. Lindorf, K. A. Mazzio, J. Pflaum, K. Nielsch, W. Brütting, M. Albrecht, *J. Mater. Chem. A* **2020**, *8*, 7495; e) W. Zhao, J. Ding, Y. Zou, C. A. Di, D. Zhu, *Chem. Soc. Rev.* **2020**, *49*, 7210; f) M. Massetti, F. Jiao, A. J. Ferguson, D. Zhao, K. Wijeratne, A. Würger, J. L. Blackburn, X. Crispin, S. Fabiano, *Chem. Rev.* **2021**, *121*, 12465; g) L. Deng, Y. Liu, Y. Zhang, S. Wang, P. Gao, *Adv. Funct. Mater.* **2023**, *33*, 2210770; h) S. H. K. Paleti, Y. Kim, J. Kimpel, M. Craighero, S. Haraguchi, C. Müller, *Chem. Soc. Rev.* **2024**, *53*, 1702.

[3] a) M. Goel, M. Thelakkat, *Macromolecules* **2020**, *53*, 3632; b) O. Bubnova, X. Crispin, *Energy Environ. Sci.* **2012**, *5*, 9345; c) F. Zhang, C.-a. Di, *Chem. Mater.* **2020**, *32*, 2688; d) O. Zapata-Arteaga, A. Perevedentsev, S. Marina, J. Martin, J. S. Reparaz, M. Campoy-Quiles, *ACS Energy Lett.* **2020**, *5*, 2972.

[4] a) L. Zhang, X.-L. Shi, Y.-L. Yang, Z.-G. Chen, *Mater. Today* **2021**, *46*, 62; b) I. H. Eryilmaz, Y.-F. Chen, G. Mattana, (Eds.: P. Cosseddu, M. Caironi), *E. Orgiu in 11 – Flexible Organic Thermoelectric Generators*, Woodhead Publishing, Sawston, Cambridge **2021**, pp. 335–351; c) Z. Liu, G. Chen, *Adv. Mater. Technol.* **2020**, *5*, 2000049; d) J.-H. Bahk, H. Fang, K. Yazawa, A. Shakouri, *J. Mater. Chem. C* **2015**, *3*, 10362.

[5] a) M. Ashizawa, Y. Zheng, H. Tran, Z. Bao, *Prog. Polym. Sci.* **2020**, *100*, 101181; b) Z. U. Khan, J. Edberg, M. M. Hamedi, R. Gabrielsson, H. Granberg, L. Wågberg, I. Engquist, M. Berggren, X. Crispin, *Adv. Mater.* **2016**, *28*, 4556; c) N. Kim, S. Lienemann, I. Petsagkourakis, D. Alemu Mengistie, S. Kee, T. Ederth, V. Gueskine, P. Leclere, R. Lazzaroni, X. Crispin, K. Tybrandt, *Nat. Commun.* **2020**, *11*, 1424; d) Q.-B. Zheng, Y.-C. Lin, Y.-T. Lin, Y. Chang, W.-N. Wu, J.-M. Lin, S.-H. Tung, W.-C. Chen, C.-L. Liu, *Chem. Eng. J.* **2023**, *472*, 145121.

[6] a) Z. B. Henson, K. Mullen, G. C. Bazan, *Nat. Chem.* **2012**, *4*, 699; b) X. Guo, M. Baumgarten, K. Müllen, *Prog. Polym. Sci.* **2013**, *38*, 1832; c) M. Kim, S. U. Ryu, S. A. Park, K. Choi, T. Kim, D. Chung, T. Park, *Adv. Funct. Mater.* **2020**, *30*, 1904545; d) H. Bronstein, C. B. Nielsen, B. C. Schroeder, I. McCulloch, *Nat. Rev. Chem.* **2020**, *4*, 66.

[7] a) M. Berggren, D. Nilsson, N. D. Robinson, *Nat. Mater.* **2007**, *6*, 3; b) H. Minemawari, T. Yamada, H. Matsui, J. y. Tsutsumi, S. Haas, R. Chiba, R. Kumai, T. Hasegawa, *Nature* **2011**, *475*, 364; c) G. Wang, W. Huang, N. D. Eastham, S. Fabiano, E. F. Manley, L. Zeng, B. Wang, X. Zhang, Z. Chen, R. Li, R. P. H. Chang, L. X. Chen, M. J. Bedzyk, F. S. Melkonyan, A. Facchetti, T. J. Marks, *Proc. Natl. Acad. Sci., U. S. A.* **2017**, *114*, E10066; d) F. Molina-Lopez, T. Z. Gao, U. Kraft, C. Zhu, T. Öhlund, R. Pfattner, V. R. Feig, Y. Kim, S. Wang, Y. Yun, Z. Bao, *Nat. Commun.* **2019**, *10*, 2676; e) C.-Y. Yang, M.-A. Stoeckel, T.-P. Ruoko, H.-Y. Wu, X. Liu, N. B. Kolhe, Z. Wu, Y. Puttisong, C. Musumeci, M. Massetti, H. Sun, K. Xu, D. Tu, W. M. Chen, H. Y. Woo, M. Fahlman, S. A. Jenekhe, M. Berggren, S. Fabiano, *Nat. Commun.* **2021**, *12*, 2354; f) I. Brunetti, F. Ferrari, N. J. Pataki, S. Abdolhosseinzadeh, J. Heier, L. J. A. Koster, U. Lemmer, M. Kemerink, M. Caironi, *Adv. Mater. Technol.* **2024**, *9*, 2302058.

[8] a) I. Petsagkourakis, K. Tybrandt, X. Crispin, I. Ohkubo, N. Satoh, T. Mori, *Sci. Technol. Adv. Mater.* **2018**, *19*, 836; b) Y. Zhang, W. Wang, F. Zhang, K. Dai, C. Li, Y. Fan, G. Chen, Q. Zheng, *Small* **2022**, *18*, 2104922; c) Y. Zhang, P. Gao, *Molecules* **2022**, *27*, 7590; d) J. P. Jurado, B. Dörling, O. Zapata-Arteaga, A. Roig, A. Mihi, M. Campoy-Quiles, *Adv. Energy Mater.* **2019**, *9*, 1902385; e) N. Pataki, P. Rossi, M. Caironi, *Appl. Phys. Lett.* **2022**, *121*, 230501.

[9] a) Z. Qiu, B. A. G. Hammer, K. Müllen, *Prog. Polym. Sci.* **2020**, *100*, 101179; b) K. Müllen, U. Scherf, *Macromol. Chem. Phys.* **2023**, *224*, 2200337.

[10] a) J. Tang, Y.-H. Pai, Z. Liang, *ACS Energy Lett.* **2022**, *7*, 4299; b) S. Wang, G. Zuo, J. Kim, H. Sirringhaus, *Prog. Polym. Sci.* **2022**, *129*, 101548; c) K. A. Peterson, E. M. Thomas, M. L. Chabinyc, *Annu. Rev. Mater. Res.* **2020**, *50*, 551; d) C. Xu, D. Wang, *Nano Lett.* **2024**, *24*, 1776.

[11] a) P. Durand, H. Zeng, T. Biskup, V. Vijayakumar, V. Untilova, C. Kiefer, B. Heinrich, L. Herrmann, M. Brinkmann, N. Leclerc, *Adv. Energy Mater.* **2022**, *12*, 2103049; b) S. E. Yoon, Y. Kang, J. Im, J. Lee, S. Y. Lee, J. Park, Y. J. Gao, D. Jeon, J. Y. Son, J. Kim, C. J. Kousseff, T. Kim, H. Seo, K. Kang, I. McCulloch, S. K. Kwak, H. H. Choi, B.-G. Kim, J. H. Kim, *Joule* **2023**, *7*, 2291; c) A. Dash, S. Guchait, D. Scheunemann, V. Vijayakumar, N. Leclerc, M. Brinkmann, M. Kemerink, *Adv. Mater.* **2024**, *36*, 2311303; d) W. Jin, C.-Y. Yang, R. Pau, Q. Wang, E. K. Tekelenburg, H.-Y. Wu, Z. Wu, S. Y. Jeong, F. Pitzalis, T. Liu, Q. He, Q. Li, J.-D. Huang, R. Kroon, M. Heeney, H. Y. Woo, A. Mura, A. Motta, A. Facchetti, M. Fahlman, M. A. Loi, S. Fabiano, *Nature* **2024**, *630*, 96.

[12] a) J. Chen, W. Zhang, L. Wang, G. Yu, *Adv. Mater.* **2023**, *35*, 2210772; b) D. Chlebosz, W. Goldeman, K. Janus, M. Szuster, A. Kiersnowski, *Molecules* **2023**, *28*, 2940.

[13] a) J. J. Michels, K. Zhang, P. Wucher, P. M. Beaujuge, W. Pisula, T. Marszalek, *Nat. Mater.* **2021**, *20*, 68; b) O. Yildiz, Z. Wang, M. Borkowski, G. Fytas, P. W. M. Blom, J. J. Michels, W. Pisula, T. Marszalek, *Adv. Funct. Mater.* **2022**, *32*, 2107976.

[14] D. Zhou, H. Zhang, H. Zheng, Z. Xu, H. Xu, H. Guo, P. Li, Y. Tong, B. Hu, L. Chen, *Small* **2022**, *18*, 2200679.

[15] a) Y. Lu, J.-Y. Wang, J. Pei, *Chem. Mater.* **2019**, *31*, 6412; b) B. Meng, J. Liu, L. Wang, *Nano Mater. Sci.* **2020**, *3*, 113.

[16] W.-N. Wu, Q.-B. Zheng, C.-L. Liu, *Synth. Met.* **2024**, *307*, 117682.

[17] a) T. L. D. Tam, J. Xu, *J. Mater. Chem. A* **2021**, *9*, 5149; b) M. Li, Y. Shi, *ChemPlusChem* **2023**, *88*, 202300215.

[18] P. Wei, J. H. Oh, G. Dong, Z. Bao, *J. Am. Chem. Soc.* **2010**, *132*, 8852.

[19] T. H. Reilly, III, A. W. Hains, H.-Y. Chen, B. A. Gregg, *Adv. Energy Mater.* **2012**, *2*, 455.

[20] B. Russ, M. J. Robb, F. G. Brunetti, P. L. Miller, E. E. Perry, S. N. Patel, V. Ho, W. B. Chang, J. J. Urban, M. L. Chabinyc, C. J. Hawker, R. A. Segalman, *Adv. Mater.* **2014**, *26*, 3473.

[21] J. Duan, J. Ding, D. Wang, X. Zhu, J. Chen, G. Zhu, C. Chen, Y. Yu, H. Liao, Z. Li, C.-a. Di, W. Yue, *Adv. Sci.* **2023**, *10*, 2204872.

[22] Y. Liu, C. Wang, T. Wang, F. Jiao, S. Dong, Y. Deng, Y. Geng, *Chin. J. Chem* **2024**, *42*, 997.

[23] a) J. Liu, B. van der Zee, R. Alessandri, S. Sami, J. Dong, M. I. Nugraha, A. J. Barker, S. Rousseva, L. Qiu, X. Qiu, N. Klasen, R. C. Chiechi, D. Baran, M. Caironi, T. D. Anthopoulos, G. Portale, R. W. A. Havenith, S. J. Marrink, J. C. Hummelen, L. J. A. Koster, *Nat. Commun.* **2020**, *11*, 5694; b) D. Yuan, D. Huang, S. M. Rivero, A. Carreras, C. Zhang, Y. Zou, X. Jiao, C. R. McNeill, X. Zhu, C.-a. Di, D. Zhu, D. Casanova, J. Casado, *Chem* **2019**, *5*, 964.

[24] a) A. Can, I. Deneme, G. Demirel, H. Usta, *ACS Appl. Mater. Interfaces* **2023**, *15*, 41666; b) I. Deneme, T. A. Yıldız, N. Kayaci, H. Usta, *J. Mater. Chem. C* **2024**, *12*, 3854.

[25] R. Ozdemir, D. Choi, M. Ozdemir, H. Kim, S. T. Kostakoğlu, M. Erkartal, H. Kim, C. Kim, H. Usta, *ChemPhysChem* **2017**, *18*, 850.

[26] H. Wei, P. A. Chen, J. Guo, Y. Liu, X. Qiu, H. Chen, Z. Zeng, T. Q. Nguyen, Y. Hu, *Adv. Funct. Mater.* **2021**, *31*, 2102768.

[27] M. Arvind, C. E. Tait, M. Guerrini, J. Krumland, A. M. Valencia, C. Cocchi, A. E. Mansour, N. Koch, S. Barlow, S. R. Marder, J. Behrends, D. Neher, *J. Phys. Chem. B* **2020**, *124*, 7694.

[28] J. Guo, Y. Liu, P.-A. Chen, X. Wang, Y. Wang, J. Guo, X. Qiu, Z. Zeng, L. Jiang, Y. Yi, S. Watanabe, L. Liao, Y. Bai, T.-Q. Nguyen, Y. Hu, *Adv. Sci.* **2022**, *9*, 2203111.

[29] M. L. Tietze, J. Benduhn, P. Pahner, B. Nell, M. Schwarze, H. Kleemann, M. Krammer, K. Zojer, K. Vandewal, K. Leo, *Nat. Commun.* **2018**, *9*, 1182.

[30] J. Kim, X. Ren, Y. Zhang, D. Fazzi, S. Manikandan, J. W. Andreasen, X. Sun, S. Ursel, H.-I. Un, S. Peralta, M. Xiao, J. Town, A. Marathianos, S. Roesner, T.-T. Bui, S. Ludwigs, H. Sirringhaus, S. Wang, *Adv. Sci.* **2023**, *10*, 2303837.

[31] a) C. Dong, B. Meng, J. Liu, L. Wang, *ACS Appl. Mater. Interfaces* **2020**, *12*, 10428; b) C. Dong, S. Deng, B. Meng, J. Liu, L. Wang, *Angew. Chem., Int. Ed.* **2021**, *60*, 16184.

[32] B. D. Naab, S. Guo, S. Olthof, E. G. Evans, P. Wei, G. L. Millhauser, A. Kahn, S. Barlow, S. R. Marder, Z. Bao, *J. Am. Chem. Soc.* **2013**, *135*, 15018.

[33] S. R. Marder, S. Barlow, *Chem. Phys. Rev.* **2024**, *5*, 021303.

[34] O. Bardagot, C. Aumaître, A. Monmagnon, J. Pécaut, P.-A. Bayle, R. Demadrille, *Appl. Phys. Lett.* **2021**, *118*, 203904.

[35] C. G. Tang, K. Hou, W. L. Leong, *Chem. Mater.* **2024**, *36*, 28.

[36] a) S. Griggs, A. Marks, H. Bristow, I. McCulloch, *J. Mater. Chem. C* **2021**, *9*, 8099; b) S. Wang, T. P. Ruoko, G. Wang, S. Riera-Galindo, S. Hultmark, Y. Puttisong, F. Moro, H. Yan, W. M. Chen, M. Berggren, C. Muller, S. Fabiano, *ACS Appl. Mater. Interfaces* **2020**, *12*, 53003.

[37] D. Yuan, W. Liu, X. Zhu, *Chem. Soc. Rev.* **2023**, *52*, 3842.

[38] W. Liu, L. Müller, S. Ma, S. Barlow, S. R. Marder, W. Kowalsky, A. Köhn, R. Lovrincic, *J. Phys. Chem. C* **2018**, *122*, 27983.

[39] a) A. Hamidi-Sakr, L. Biniek, J.-L. Bantignies, D. Maurin, L. Herrmann, N. Leclerc, P. Lévêque, V. Vijayakumar, N. Zimmermann, M. Brinkmann, *Adv. Funct. Mater.* **2017**, *27*, 1700173; b) P. A. Gilhooly-Finn, I. E. Jacobs, O. Bardagot, Y. Zaffar, A. Lemaire, S. Guchait, L. Zhang, M. Freeley, W. Neal, F. Richard, M. Palma, N. Banerji, H. Sirringhaus, M. Brinkmann, C. B. Nielsen, *Chem. Mater.* **2023**, *35*, 9029; c) S. Wang, W. Zhu, I. E. Jacobs, W. A. Wood, Z. Wang, S. Manikandan, J. W. Andreasen, H.-I. Un, S. Ursel, S. Peralta, S. Guan, J.-C. Grivel, S. Longuemart, H. Sirringhaus, *Adv. Mater.* **2024**, *36*, 2314062.

[40] a) J. Mei, D. H. Kim, A. L. Ayzner, M. F. Toney, Z. Bao, *J. Am. Chem. Soc.* **2011**, *133*, 20130; b) X. Cao, H. Li, J. Hu, H. Tian, Y. Han, B. Meng, J. Liu, L. Wang, *Angew. Chem., Int. Ed.* **2023**, *62*, e202212979.

[41] S. K. Yee, N. E. Coates, A. Majumdar, J. J. Urban, R. A. Segalman, *Phys. Chem. Chem. Phys.* **2013**, *15*, 4024.

[42] L. Qiu, J. Liu, R. Alessandri, X. Qiu, M. Koopmans, R. W. A. Havenith, S. J. Marrink, R. C. Chiechi, L. J. Anton Koster, J. C. Hummelen, *J. Mater. Chem. A* **2017**, *5*, 21234.

[43] C. Y. Yang, Y. F. Ding, D. Huang, J. Wang, Z. F. Yao, C. X. Huang, Y. Lu, H. I. Un, F. D. Zhuang, J. H. Dou, C. A. Di, D. Zhu, J. Y. Wang, T. Lei, J. Pei, *Nat. Commun.* **2020**, *11*, 3292.

[44] C. Adamo, V. Barone, *J. Chem. Phys.* **1999**, *110*, 6158.

[45] V. A. Rassolov, M. A. Ratner, J. A. Pople, P. C. Redfern, L. A. Curtiss, *J. Comput. Chem.* **2001**, *22*, 976.